Organic Electronics 12 (2011) 269–278

Contents lists available at ScienceDirect

Organic Electronics

journal homepage: www.elsevier.com/locate/orgel

Photoreactive low-bandgap 4*H*-cyclopenta[2,1-b:3,4-b′]dithiophene and 4,7-di(thiophen-2-yl)benzo[c][1,2,5]thiadiazole-based alternating copolymer for polymer solar cell

U Ra Lee [a], Tae Wan Lee [a], Mai Ha Hoang [a], Nam Su Kang [b], Jae Woong Yu [c], Kyung Hwan Kim [a], Kyung-Geun Lim [d], Tae-Woo Lee [d], Jung-Il Jin [a], Dong Hoon Choi [a,*]

[a] Department of Chemistry, Research Institute for Natural Sciences, Korea University, 5 Anam-dong, Sungbuk-gu, Seoul 136-701, Republic of Korea
[b] Korea Institute of Science & Technology, Center for Energy Materials Research, 39-1 Hawolkok-dong, Sungbuk-gu, Seoul 136-791, Republic of Korea
[c] Advanced Materials Engineering for Information and Electronics, Kyung Hee University, 1 Seocheon, Kiheung, Yongin, Kyungki 446-701, Republic of Korea
[d] Department of Materials Science and Engineering, Pohang University of Science and Technology, Pohang, Gyungbuk 790-784, Republic of Korea

ARTICLE INFO

Article history:
Received 29 July 2010
Received in revised form 20 November 2010
Accepted 22 November 2010
Available online 5 December 2010

Keywords:
Low-bandgap polymer
Photoreaction
Bulk heterojunction
Long-term stability
Polymer solar cell

ABSTRACT

Polymer solar cells (PSCs) are often fabricated using a well-known 4*H*-cyclopenta[2,1-b:3,4-b′]dithiophene and 4,7-di(thiophen-2-yl)benzo[c][1,2,5]thiadiazole-based polymer as a low-bandgap polymer. Further, PSCs are also fabricated by mixing methanofullerene [6,6]-phenyl C61-butyric acid methyl ester ($PC_{61}BM$) with the polymer. We prepared poly[4,4-bis(2-ethylhexyl)-4*H*-cyclopenta[2,1-b:3,4-b′]dithiophene-2,6-diyl-alt-4,7-bis(2-thienyl)-2,1,3-benzothiadiazole-5′,5″-diyl] after anchoring the penta-1,4-diene in the side chain of the cyclopentadithiophene and investigated the long-term performance stability of a photocrosslinked bulk heterojunction (BHJ) photovoltaic (PV) cell based on the polymer. The photocrosslinking reaction was monitored via infrared spectroscopy without the use of a photoinitiator, by carrying out a spontaneous radical coupling reaction. The polymer film has a broad absorption band extending from 300 to 850 nm with an optical bandgap as low as 1.52 eV. The polymer was employed to fabricate a PSC with $PC_{61}BM$. The resultant PSC device, which was treated by UV irradiation ($\lambda = 254$ nm, $I = 40$ mW/cm^2, 5 min), had good preliminary results with an open-circuit voltage of 0.62 V, a short-circuit current density of -5.37 mA/cm^2, a fill factor of 0.41, and an overall power conversion efficiency of 1.37%. All parameters of the UV-cured PSC device were more stable over the course of 300 h than those of P3HT-$PC_{61}BM$ devices, indicating the long-term stability of the polymer.

1. Introduction

Substantial progress has been made in the exploration of organic semiconductors as active elements in electronic devices such as light-emitting diodes, thin-film transistors (TFTs), and solar cells [1–7]. With regard to the application of organic semiconductors in electronic and optoelectronic devices, the organic photovoltaic (OPV) cell is expected to play an important role in developing devices to meet future energy requirements [8–15].

Bulk heterojunction (BHJ) PSCs have been shown to be the most promising devices for OPV cells. PSCs made of regioregular poly(3-hexylthiophene), poly[p-phenylene vinylene] and polyfluorene derivatives have been demonstrated with [6,6]-phenyl C (61 or 71) butyric acid methyl ester (PCBM) and exhibited quite promising power conversion efficiency (PCE) [16–22]. Since the photon flux of the solar emission has a maximum at 680 nm, many promising low-bandgap polymers have been designed and reported in the literatures [23–26].

* Corresponding author. Tel.: +82 2 3290 3140; fax: +82 2 924 3141.
E-mail address: dhchoi8803@korea.ac.kr (D.H. Choi).

1566-1199/$ - see front matter © 2010 Elsevier B.V. All rights reserved.
doi:10.1016/j.orgel.2010.11.021

The PCE value is often considered to evaluate device functionality and material properties in the PSC devices. The durability of PCEs, however, has not been much discussed. In fact, the lifetime of PSC is relatively short compared to silicon-based solar cells. In order to achieve good performance stability of PSC devices, the blend morphology of donor and acceptor materials should be sufficiently stable. Kim et al. emphasized the importance of the stability of the blend morphology in enabling the practical application of well-known BHJ PV devices, because any heat generated by solar emission can be detrimental to the performance of the devices. This damage is a result of the relatively low glass transition temperature (T_g) of the polymer blend and the miscibility of donor and acceptor materials in the photoactive layer [27]. Several useful methods for improving the performance stability of PSCs have been suggested in the literature, including the use of a proper compatibilizer and a fixation process involving two materials that stabilizes the two phases after nanophase separation [28]. Thermal crosslinking reactions have also been adopted to improve the stability of the blend morphology. However, thermal treatments used to induce crosslinking may be detrimental in that they prevent the annealing processes from being properly carried out [29–31]. Consequently, one of the major goals of this research is to control such "trade-off" problems.

In order to achieve this goal, we employed a photocrosslinking reaction to activate the thermal annealing process, followed by a separate photocrosslinking reaction. Considering all of the requirements for a photocrosslinkable BHJ, we designed a new copolymer based on a known low-bandgap polymer employing penta-1,4-diene, which undergoes a spontaneous photoreaction without the need for a photoinitiator. We hypothesized that the blend morphology would be tightly confined in three-dimensions following photocrosslinking as a result of volume shrinkage. The acceptor materials inside the polymer were expected to be more tightly caged by reducing the free volume through a lattice hardening mechanism. We also sought to control the stability of the interfacial contact between the materials by maintaining the semiconducting molecular nature and intrinsic electronic properties of the polymer.

The structures of the low-bandgap host polymers were designed such that the donor and acceptor moieties could be combined in the repeating unit in an alternating fashion. The electronic molecular energy levels (e.g., HOMO and LUMO levels) can be controlled through the intramolecular charge transfer (ICT) in D–A alternating copolymers.

In this study, we report the synthesis of the 4,7-di(thiophen-2-yl)benzo[c][1,2,5]thiadiazole (or 4,7-bis(thien-2-yl)-2,1,3-benzothiazole) and 4*H*-cyclopenta[2,1-b:3,4-b′]dithiophene-based copolymer using an alternating heteroarene-fused π-conjugated system containing bis(heptyl penta-1,4-dien-3-yl succinate) in the repeating unit. The feasibility of the polymer for fabricating PSC devices was investigated. In addition, the polymer was mixed with $PC_{61}BM$ to fabricate BHJ PSC devices. For comparative purposes, we also fabricated a control device, i.e., P3HT/$PC_{61}BM$ (1:2 w/w, η = 3.7–4.0%). The thermally annealed and UV-cured samples had an average PCE of 1.37% in OPV devices. The photocured BHJ PSC device fabricated using the new photoreactive polymer showed a significant improvement in stability relative to that of the BHJ fabricated with P3HT/$PC_{61}BM$ over a duration of 300 h.

2. Experimental

2.1. Materials

All commercially available starting materials and solvents were purchased from Aldrich, TCI, and ACROS Co. and used without further purification unless otherwise stated. HPLC grade toluene, methylene chloride (MC), Dimethylsulfoxide (DMSO) and tetrahydrofuran (THF) were purchased from J.T. Baker and distilled from CaH_2 immediately before use.

We synthesized 4*H*-cyclopenta[2,1-b:3,4-b′]dithiophene, **1** [32], 4,7-bis(2-bromo-5-thienyl)-2,1,3-benzothiazole, **5** [33] by following the literature method. Poly(3-hexylthiophene) and $PC_{61}BM$ was purchased from Rieke Metals and Nano-C, respectively.

2.2. Synthesis

2.2.1. (6-Bromohexyloxy)(tert-butyl)dimethylsilane (2)

6-Bromo-1-hexanol (11 g, 61 mmol), imidazole (12 g, 182 mmol), and 4-dimethylaminopyridine (DMAP, 0.74 g, 6.1 mmol) were mixed in 100 mL of MC under argon gas purging in a 250 mL three necked flask. *tert*-Butylchlorodimethylsilane (TBDMSCl, 18 g, 121 mmol) was added into the mother solution and the solution was allowed to stand for 3 h. Next, 10 mL of deionized water was added to quench the reaction. The mixture was extracted with MC (100 mL) and water (300 mL). The organic layer was collected and dried with sodium sulfate (Na_2SO_4). After concentrating the solution, the crude product was purified by silica gel column chromatography (eluent; ethyl acetate: *n*-hexane = 1:3). The reaction produced 14 g of product (**2**) (yield: 78%).

^{1}H NMR (300 MHz, CDC13): δ(ppm) 3.60 (t, J = 6.3, 2H), 3.40 (t, J = 6.9, 2H), 1.86 (q, J = 5.1, 2H), 1.54–1.35 (m, 6H), 0.89 (s, 9H), 0.04 (s, 6H) ^{13}C NMR (CDC13): δ(ppm) 63.0, 33.8, 32.8, 32.6, 27.9, 25.9, 25.0, 18.3, 5.3.

2.2.2. 4,4′-Bis(((tert-butyl)dimethylsilyloxy)hexyl)dicyclopenta[2,1-b:3,4-b′]dithiophene (3)

Compound (**1**) (1.5 g, 8.4 mmol) was dissolved in 70 mL dimethylsulfoxide (DMSO) at 0 °C and the solution was allowed to stir for 10 min under an argon atmosphere after the addition of KOH (1.5 g, 27 mmol) and KI (35 mg, 0.21 mmol). Compound (**2**) (6.2 g, 21 mmol) was added into the mother solution and the reaction was kept at 25 °C for 24 h. The reaction mixture was extracted with MC (100 mL) and water (300 mL). The organic layer was collected and dried with Na_2SO_4. The concentrated solution was purified by silica gel column chromatography (eluent; ethyl acetate: *n*-hexane = 1:3), yielding product **3**, 3.4 g (yield: 66%).

^{1}H NMR (300 MHz, CDC13): δ(ppm) 7.14 (d, J = 4.68 Hz, 2H), 6.91 (d, J = 4.68 Hz, 2H), 3.51 (t, J = 6.6, 4H), 1.81 (m, J = 5.1, 4H), 1.41–1.13 (m, 16H), 0.87 (s, 18H), 0.01 (s, 12H) ^{13}C NMR (CDC13): δ(ppm) 157.9, 136.4, 124.4, 121.5, 67.9, 63.2, 53.1, 37.6, 32.7, 29.7, 25.9, 24.4, 25.5, 18.3, 5.3.

EA analysis calcd. for C33H58O2S2Si2: C, 65.28; H, 9.63; S, 10.58; found: C, 65.37; H, 9.23; S, 10.90.

*2.2.3. 2,6-Di(tributyltin)-4,4′-bis((tert-butyl)dimethylsilyl)hexyl)dicyclopenta[2,1-b:3,4-b′]dithiophene (**4**)*

Compound (**3**) (3 g, 5 mmol) was dissolved in 70 mL of THF at 25 °C in a 250 mL round bottom flask and the solution was kept under an argon atmosphere. Next, *n*-butyllithium (2.5 M) in *n*-hexane (50 mL, 20 mmol) was added using a microsyringe. After the addition was completed, the reaction mixture was allowed to stir for 1 h, and then tributyltin chloride (6.4 g, 20 mmol) was added. After 6 h, the mixture was extracted with MC (200 mL) and water (400 mL). The organic layer was dried with Na_2SO_4 and the solution was concentrated. The crude product was purified by silica gel column chromatography treated with triethylamine (eluent; chloroform: *n*-hexane = 1:1) to produce 4.57 g of compound **4** (yield: 78%).

^{1}H NMR (300 MHz, CDC13): δ(ppm) 6.87 (s, 2H), 3.52 (t, J = 6.6, 4H), 1.72 (m, 4H), 1.10–1.50 (m, 24H), 0.80–1.00 (m, 30H), 0.87 (s, 9H), 0.01 (s, 6H) ^{13}C NMR (CDC13): δ(ppm) 160.1, 142.2, 135.8, 129.6, 63.2, 51.9, 37.7, 32.8, 29.8, 29.2, 28.9, 27.1, 25.9, 25.6, 24.6, 18.36, 13.6, 10.8, 8.7.

EA analysis calcd. for C57H110O2S2Si2Sn2: C, 57.76; H, 9.35; S, 5.41; found: C, 57.91; H, 9.07; S, 5.55.

*2.2.4. Polymer (**6**)*

Compound (**4**) (2.3 g, 1.9 mmol) and compound (**5**) (0.87 g, 1.9 mmol) were dissolved in 70 mL of toluene under an argon atmosphere. After adding $Pd(PPh_3)_4$ (0.11 g, 0.09 mmol), the reaction mixture was heated to 90 °C and stirred for 48 h. An End-capping reaction was performed by adding a toluene solution (5 mL) of tributyl tin thiophene (400 mg, 1.1 mmol). 2-Bromothiophene (800 mg, 4.9 mmol) in 5 mL of toluene was added dropwise into the mother solution. The reaction mixture was cooled to room temperature and was added dropwise into 60 mL of methanol to precipitate the crude solid product. The crude product was purified by Soxhlet extraction with methanol and acetone. The solid product was dissolved in 20 mL of chloroform and precipitation was performed in 300 mL of methanol again. The product was filtered and dried under vacuum for 48 h. Finally, 0.95 g of a dark blue solid powder (**6**) was obtained (yield: 53%).

^{1}H NMR (300 MHz, CDC13): δ(ppm) 7.89–6.98 (8H), 3.56 (s, br, 4H), 1.85 (s, br, 4H), 1.45–1.24 (m, 16H), 0.89 (s, 18H), 0.04 (s, 12H) GPC (THF): M_n = 3886 g/mol, M_w = 10,705 g/mol, PDI = 2.75 EA analysis calcd. for C47H64N2S5Si2: C, 62.34; H, 7.12; N, 3.09; S, 17.71; found: C, 62.88; H, 7.31; N, 3.55; S, 17.31.

*2.2.5. Polymer (**7**)*

Polymer **6** (0.4 g, 0.43 mmol) was dissolved in THF (70 mL) containing HCl (0.86 g, 8.6 mmol). The reaction was kept at room temperature for 48 h. After checking the progress of the reaction by thin layer chromatography, the reaction was neutralized with triethylamine. After concentrating the solution, the solution was dissolved into 300 mL methanol for precipitation. The crude product was filtered and dried under vacuum for 48 h. After drying, 0.25 g of a dark brown solid, compound (**7**), was obtained (yield: 83%).

EA analysis calcd. for C35H36N2O2S5: C, 62.09; H, 5.36; N, 4.14; S, 23.68; found: C, 62.92; H, 5.67; N, 3.80; S, 22.27.

2.2.6. Photoreactive polymer 8

Polymer **7** (0.2 g, 0.28 mmol) was dissolved in 80 mL of THF and 30 mL of MC. Dicyclohexyl carbodiimide (DCC, 0.15 g, 0.71 mmol) and DMAP (35 mg, 0.28 mmol) were added successively. 4-Oxo-4-(penta-1,4-dien-3-yloxy)butanoic acid (0.30 g, 1.4 mmol) was introduced into the mother solution and the solution was allowed to stand for 24 h. The residual hydroxyl group was protected with acetyl chloride. After the reaction was complete, the solid was purified by Soxhlet extraction with methanol and acetone successively. The solid was dissolved in chloroform again and precipitation was performed in methanol. The solid was filtered and dried under vacuum for 48 h. A dark blue solid polymer, compound **8**, was obtained (0.21 g, yield: 72%).

^{1}H NMR (300 MHz, CDC13): δ(ppm) 7.89–6.93 (8H), 5.79 (m, 4H), 5.70 (t, 2H), 5.23 (m, 8H), 4.02 (s, br, 4H), 2.63 (s, br, 8H), 1.92 (s, br, 4H), 1.27 (m, br, 16H) GPC (THF): M_n = 5991 g/mol, M_w = 20,431 g/mol, PDI = 3.41.

EA analysis calcd. for C53H56N2O8S5: C, 63.07; H, 5.59; N, 2.78; S, 15.88; found: C, 63.43; H, 5.33; N, 2.95; S, 15.06.

2.2.7. Instrumentation

^{1}H NMR spectra were recorded on a Varian Mercury NMR 300 MHz spectrometers using $CDCl_3$ purchased from Cambridge Isotope Laboratories, Inc. Elemental analyses were performed by the Center for Organic Reactions using an EA1112 (Thermo Electron Corp.) elemental analyzer. Thermal properties were studied under a nitrogen atmosphere on a Mettler DSC 821^e Instrument. Thermal gravimetric analysis (TGA) was conducted on a Mettler TGA50 (temperature rate 10 °C/min under N_2). The redox properties of synthesized polymers were examined by using cyclic voltammetry (Model: EA161 eDAQ). Thin films were coated on a platinum plate using methylene chloride as a solvent. The electrolyte solution employed was 0.10 M tetrabutylammonium hexafluorophosphate (Bu_4NPF_6) in a freshly dried methylene chloride (MC). The Ag/AgCl and Pt wire (0.5 mm in diameter) electrodes were utilized as reference and counter electrodes, respectively. The scan rate was at 50 mV/s. Fourier transformed-Infrared (FT-IR) spectra were recorded using a Nicolet 380 infrared spectrophotometer.

2.2.8. Absorption and PL spectroscopy

In order to study absorption behavior, the polymer film was fabricated on quartz substrates as follows. The solution (2.5 wt%) of polymer in monochlorobenzene was filtered through an acrodisc syringe filter (Millipore 0.2 μm) and subsequently spin-cast on the quartz glass.

The film was dried overnight at 80 °C for 12 h under vacuum. Absorption spectra of film samples were obtained using a UV–vis spectrometer (HP 8453, photodiode array type) in the wavelength range of 190–1100 nm.

When we investigate the PL spectral behavior, two emission spectra were recorded using the 488 nm line of a Ar^+ laser as the excitation light source. For PL measurements, the film specimen was mounted on the cold finger in the vacuum chamber (pressure < 10^{-5} Torr) of a closed cycle refrigerator. Emitted light was collected by a lens and analyzed using a single monochromator with 1 m focal length and a GaAs cathode photomultiplier. Standard lock-in detection techniques were used to maximize the signal-to-noise ratio. The diameter of incident laser beam was about 0.3 mm.

2.2.9. OTFT fabrication

Bottom-gate top-contact device geometry was employed for characterization of TFT performance. Spin-coated films (thickness ~40–50 nm) of polymer **8** were prepared on a heavily n-doped Si/SiO_2 substrate with monochlorobenzene (MCB) as solvent. Surface modification was carried out with octyltrichlorosilane (OTS) to give hydrophobic dielectric surfaces. The OTFTs were fabricated by directly spin-coating the polymer solution onto the dielectric substrate at 1200 rpm. The fabricated thin films were heated in air at 120 °C to remove the solvent and to anneal them thermally at 150 °C for 20 min. Then, the film was exposed to UV light for 5 min at 25 °C for inducing photocrosslink.

Source and drain electrodes were then thermally evaporated (t = 100 nm) through a shadow mask with a channel width and length of 1500 μm, and 100 μm, respectively. All the field effect mobilities were extracted in the saturation regime using the relationship $\mu_{sat} = (2I_{DS}L)/(WC(V_g - V_{th})^2)$, where I_{DS} is the a saturation drain current, C is the capacitance of the silicon oxide dielectric, V_g is the gate bias, and V_{th} is the threshold voltage. The device performance was evaluated in air using Keithley 4200-SCS semiconductor characterization system under ambient conditions.

2.2.10. PSC device fabrication

The hole collecting electrode was 300–400 nm thick indium tin oxide (ITO) coated glass with resistance of 19.5 Ω/cm. ITO glass was cleaned by boiling in chloroform, isopropyl alcohol, and acetone for 30 min in each solvent, sonification for 15 min in 50:50 isopropyl alcohol and acetone solution, and finally rinsed with de-ionized water. The cleaned ITO coated glass was treated with O_2 plasma and flattening ITO with a microwave-generated plasma reactor (Plasmatic Systems Inc., PLASMATIC-PREENII, 24 GHz) for 15 min. 30 nm thick PEDOT:PSS layer (Baytron P, 1 S cm^{-1}) was coated by spin coating stock solution at 2500 rpm for 30 s. PEDOT:PSS coating was heat treated in the glove box at 200 °C for 5 min.

The polymer and $PC_{61}BM$ were dissolved in anhydrous monochlorobenzene. The thickness of a resulting photoactive layer was ~80 nm. For inducing photocrosslinking, the film was exposed to UV light for 1 and 5 min. LiF (0.8 nm thick) which served as a buffer layer, was vacuum deposited on top of active layer and 150 nm thick aluminum was evaporated. Thickness of the photoactive film was measured with surface profiler (TENCOR®, P-10 α-step). Current–voltage characteristics were measures with Keithley 2400 source-measure unit. Xe lamp (300 W) was used as a light source to produce intensity of 100 mW/cm^2. To mimic sun light, AM 1.5 filter (Oriel) was used neutral density filter was used to reduce intensity as necessary. Intensity of incoming light power was measured with calibrated broadband optical power meter (Spectra Physics model 404).

3. Results and discussion

3.1. Synthesis and characterization

Scheme 1 illustrates the synthetic routes for the monomers and a π-conjugated D–A alternating copolymer having heteroaromatic-ring moieties as a repeating group. TBDMS-protected hexyl bromide was reacted with 4*H*-cyclopenta[2,1-b:3,4-b′]dithiophene to yield compound **3**. Compound **3** was then lithiated using *n*-butyllithium, with a reaction yield of 78%. Following lithiation, the tributyl tin groups were reacted with 4*H*-cyclopenta[2,1-b:3,4-b′]dithiophene in order to conduct Stille coupling polymerization. The 4,7-di(thiophen-2-yl)benzo[c][1,2,5]thiadiazole was synthesized following the method given in literature [33]. Bromination of 4,7-di(thiophen-2-yl)benzo[c][1,2,5]thiadiazole with *N*-bromosuccimide (NBS) yielded the dibromide monomer **5**. Eventually, the Stille coupling polymerization of monomer **5** was conducted with monomer **4** bearing tributylstannyl groups in the presence of a catalytic amount of $Pd(PPh_3)_4$ to afford polymer **6**. The TBDMS unit was then removed in the presence of hydrochloric acid at 25 °C. After removing the TBDMS groups from polymer **6**, the DCC esterification of polymer **7** and 4-oxo-4-(penta-1,4-dien-3-yloxy)butanoic acid produced polymer **8** in good yield (72%).

The identity and purity of the synthetic materials were confirmed by ^1H NMR, ^{13}C NMR, and elemental analysis. As solubilizing groups, tert-butyl(heptyloxy)dimethylsilane side chains were substituted in the dicyclopenta[2,1-b:3,4-b′]dithiophene groups in the polymer structures. The weight-average molecular weight (M_w) of **8** was determined by gel permeation chromatography (GPC) using a polystyrene standard and was found to be 20,431 (M_w/M_n = 3.41). The polymers **6–8** are soluble in various organic solvents including chloroform, xylene, MC, chlorobenzene, and THF, and they can be fabricated into smooth films by a spin-coating method.

The thermogravimetric analysis (TGA) measurements were conducted at a heating rate of 10 °C/min under nitrogen. The measurements revealed that the polymers were thermally stable having a decomposition temperature, T_d, of 325 °C (see Fig. 1A). The thermally induced phase transition behavior of polymer **8** was investigated with differential scanning calorimetry (DSC) under a nitrogen atmosphere. The glass transition temperature of the polymer was not detected but the melting temperature was determined to be 75 °C, indicating the semi-crystalline nature of the polymer.

FT-IR spectroscopy: An FT-IR investigation was carried out to confirm that photocrosslinking had occurred

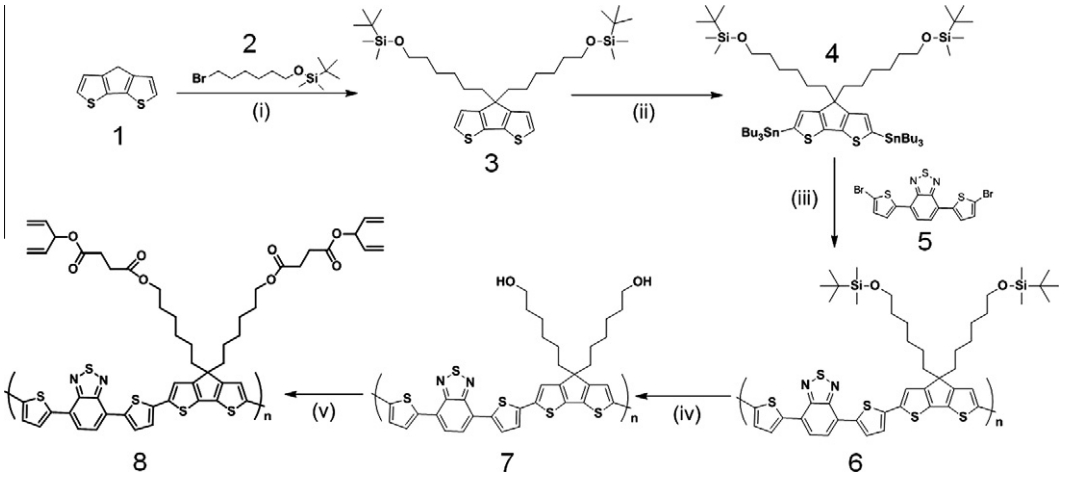

Scheme 1. Synthetic procedure for a photoreactive low-bandgap D–A alternating copolymer. (i) KOH, KI, DMSO, rt; (ii) Bu_3SnCl, *n*-BuLi, −78 °C; (iii) $Pd(pph_3)_4$, toluene, 90 °C; (iv) HCl, THF, rt; (v) 4-oxo-4-(penta-1,4-dien-3-yloxy)butanoic acid, DCC, DMAP, rt.

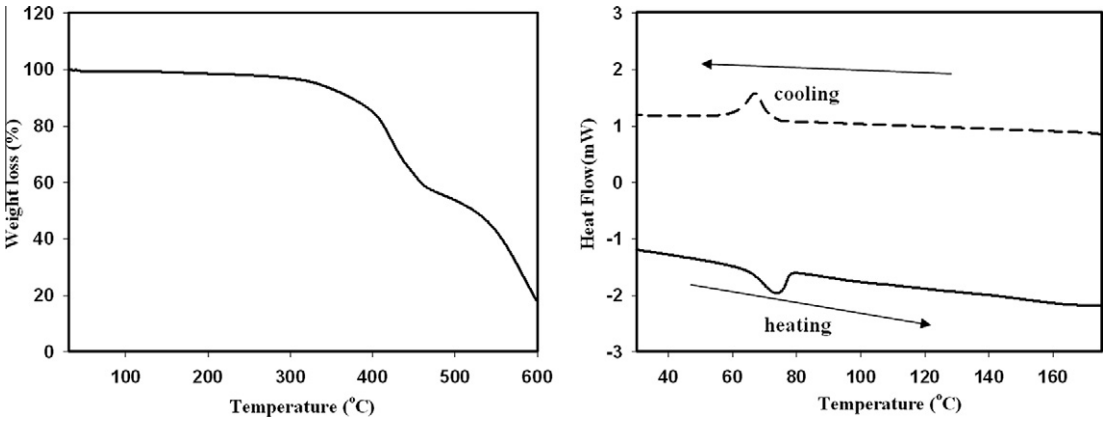

Fig. 1. TGA and DSC thermal analysis of the polymer. (A) TGA and (B) DSC.

between the pentadiene units. The film sample was prepared on a KBR window using the spin-coating method. Fig. 2 shows the FT-IR spectra of the polymer films before and after UV exposure (λ = 254 nm, I = 40.5 mW/cm^2). The characteristic absorption bands at 931, 985, and 1446 cm^{-1}, which can be unambiguously assigned to the pentadiene photoreactive groups, are labeled in the figure. The observed decrease in the intensity of the CH out-of-plane deformation in –CH=CH_2 at 985 and 931 cm^{-1} was clear evidence of the polymerization. Further verification of crosslinking was found from the slight decrease in the intensity of the in-plane deformation band of =CH at 1446 cm^{-1}.

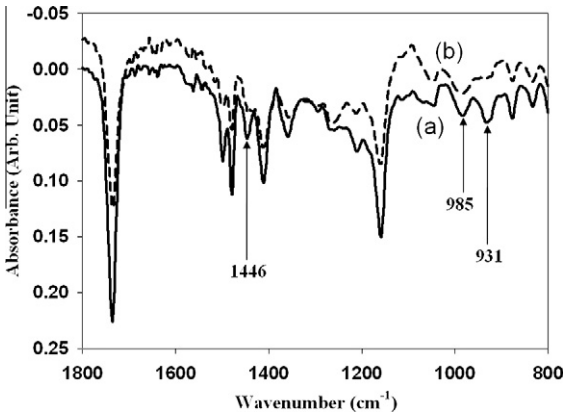

Fig. 2. FT-IR spectra of polymer **8** film before (a) and after (b) UV exposure.

3.2. Absorption and photoluminescence (PL) spectroscopy of polymer 8

The absorption spectra of polymer **8** in both dilute chloroform solution (conc. = 1 × 10^{-6} M) and thin solid films spin coated on a quartz substrate are illustrated in Fig. 3. The absorption maxima of polymer **8** and the other measured data are summarized in Table 1. In the solution state, polymer **8** exhibited absorption maxima at 657 and 446 nm and an absorption edge at 790 nm, indicating an optical

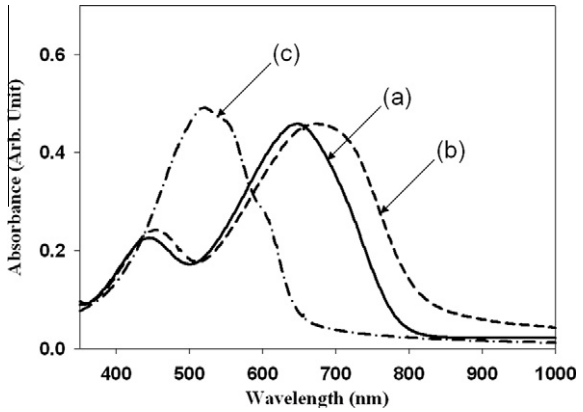

Fig. 3. Absorption spectra of polymer **8** in (a) solution and (b) film states. Spectrum (c) was obtained from P3HT film for comparison.

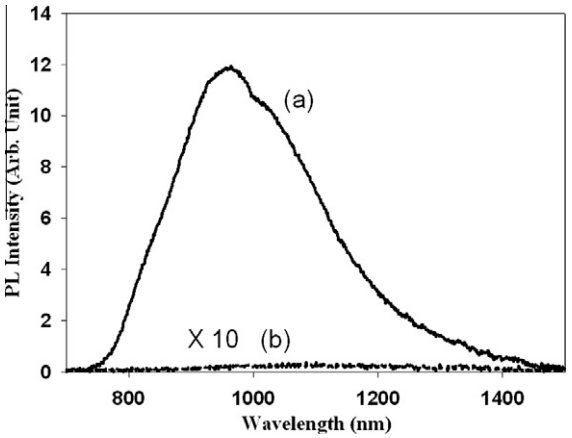

Fig. 4. PL spectra of the copolymer (a) and the blend sample with $PC_{61}BM$ (1:2 w/w) The PL intensity scale in spectrum (b) has been enlarged by 10 times.

bandgap energy of 1.52 eV. The low energy band is due to ICT between the donor and acceptor.

The absorption spectrum of the film of polymer **8** exhibits slight broadening and is red shifted by 10–12 nm compared to that of the solution state. This bathochromic shift results from strong intermolecular interactions in the solid state. The absorption maximum is hard to determine accurately, and the spectrum of the film floated over the base line, indicating the existence of scattering loss as a result of solid-state crystallization. Polymer **8** exhibits significant absorption throughout the visible region, extending into the NIR wavelength range. The optical spectrum of the film ranges from 300 to 850 nm, which can be fitted to the solar spectrum. The optical bandgap energy ($E_g^{opt.}$) in the film state was determined to be 1.52 eV, which is much smaller than that of the widely used regioregular poly(3-hexylthiophene) (P3HT) ($E_{HOMO} = -5.07$ eV, $E_{LUMO} = -3.24$ eV, $E_g^{opt.} = 1.83$ eV).

The photoluminescence (PL) spectra of the pristine film and blend film with $PC_{61}BM$ (1:2 w/w) were also acquired and are presented in Fig. 4. Because these polymers were expected to have an emission band in the near-IR region, a customized optical set-up was built to measure the emission spectrum generated by excitation at 488 nm with an Ar^+ laser. The wavelength of maximum emission is approximately 964 nm and the emission edge occurs in the region of 1500 nm, which is a typical emission spectrum for low-bandgap polymers, and corresponds to the long wavelength range of the absorption maximum.

As a representative example, the absorption spectrum of the blend sample with the copolymer and $PC_{61}BM$ (1:2 w/w) in the film state is illustrated. No emission was observed in the blended sample film (curve b) under 488 nm excitation. This PL quenching behavior can be explained by the aggregation-induced self-quenching of the excited polymer states and $PC_{61}BM$ units. The lack of emission might also be a result of intermolecular electron transfer from the photoexcited polymers to the $PC_{61}BM$ sensitizer. The photoinduced charge transfer in other conjugated molecular composites by PL quenching can be found in the literature, and is a prerequisite for efficient solar cells [34–36].

3.3. Electrochemical analysis

The electrochemical properties of the polymer were investigated by cyclic voltammetry and the scanned cyclic voltammogram is shown in Fig. 5. The HOMO and LUMO energies of the polymer are quite important for determining how to facilitate the photoinduced electron transfer in the BHJ OPV device after blending with $PC_{61}BM$. The voltammogram of a film sample was recorded and the potentials were obtained relative to an internal ferrocene reference (Fc/Fc^+).

The HOMO and LUMO levels of the polymer were estimated using the onset potentials of the oxidation and reduction waves. Polymer **8** showed one quasi-reversible oxidation peak and one quasi-reversible reduction peak. The HOMO and LUMO energy levels and electrochemical bandgap energy (E_g^{ec}) of the copolymer calculated from E_{ox}^{onset} and E_{red}^{onset} are listed in Table 1. The voltammogram

Table 1
Physical properties of polymer **8**.

	T_m (°C)	T_c (°C)	T_d (°C)	Solution		Film		E_{ox}^{onset} (V)/HOMO (eV)	E_{red}^{onset} (V)/LUMO (eV)	E_g^{ec} (eV)	E_g^{opt} (eV)
				λ_{max}^{abs} (nm)	$\lambda_{cut\text{-}off}$ (nm)	λ_{max}^{abs} (nm)	$\lambda_{cut\text{-}off}$ (nm)				
Polymer	74	67	325	446,657	785	453,669	815	0.51/−4.91	−0.85/−3.55	1.36	1.52

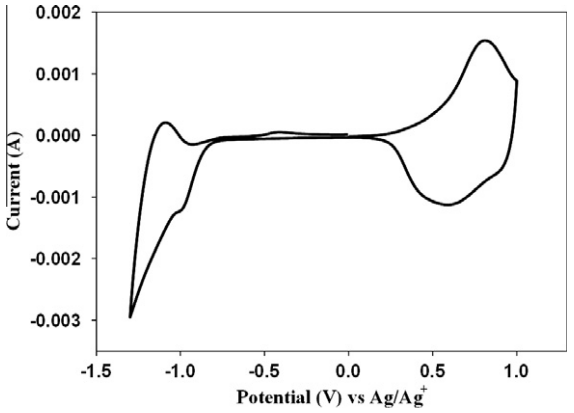

Fig. 5. Cyclic voltammogram of the polymer **8** film.

of the polymer in the film state showed that its lowest oxidative wave was at +0.51 eV. As shown in Table 1, polymer **8** has a HOMO level of −4.91 eV.

In addition, polymer **8** has a LUMO energy level of −3.55 eV. The electrochemical bandgap energy of the film sample was determined to be 1.36 eV, which is 0.06 eV less than the optical bandgap energy ($E_g^{opt.}$ = 1.52 eV). For comparison, the HOMO and LUMO levels of regioregular P3HT were also measured under identical conditions, and were found to have energies of −5.07 and −3.24 eV, respectively.

Although the HOMO level is too low to show low open-circuit voltage (V_{oc}), in the energy diagram (see Fig. 7) of the BHJ OPV devices, efficient photoinduced electron transfer between the host polymers and acceptor is expected on the basis of the PL quenching behavior.

3.4. Properties of OTFT made of polymer 8

A 40-nm-thin film of polymer **8** was deposited on OTS-SiO_2 by spin coating a 1 wt% solution of the polymer in monochlorobenzene. After spin coating the polymer solution onto the surface of the insulator, the thin-film layer (t = 70 nm) was annealed at 150 °C for 10 min and exposed to UV light (λ = 254 nm, I = 40 mW/cm^2). The gold electrodes were then deposited via thermal evaporation for the fabrication of thin-film transistors.

Fig. 6 shows the typical drain current (I_{DC}) versus source–drain voltage (V_{DS}) plots for various gate voltages

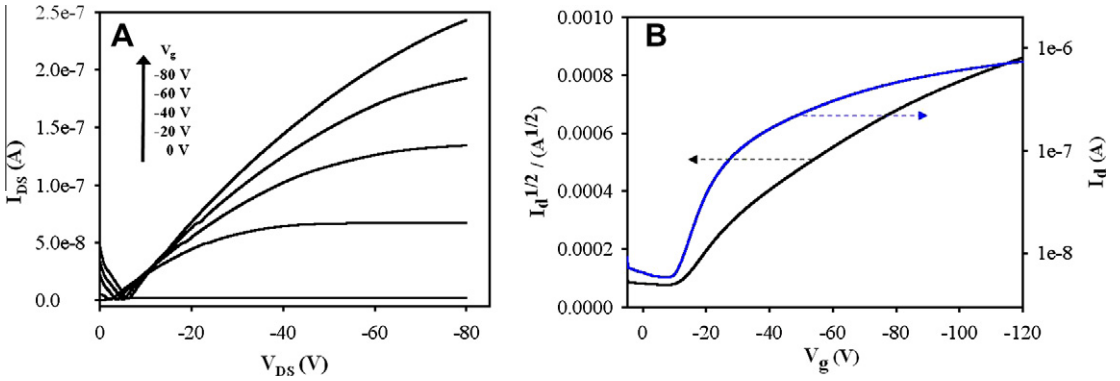

Fig. 6. Current–voltage characteristics (I_{DS} versus V_{DS}) at different gate voltages (V_g) (left) and I_{DS} and $(-I_{DS})^{1/2}$ versus V_g plots at V_{DS} of −100 V (right) for a top contact device (annealing at 150 °C, W = 1.5 mm, L = 100 μm). Insulator: OTS treated SiO_2.

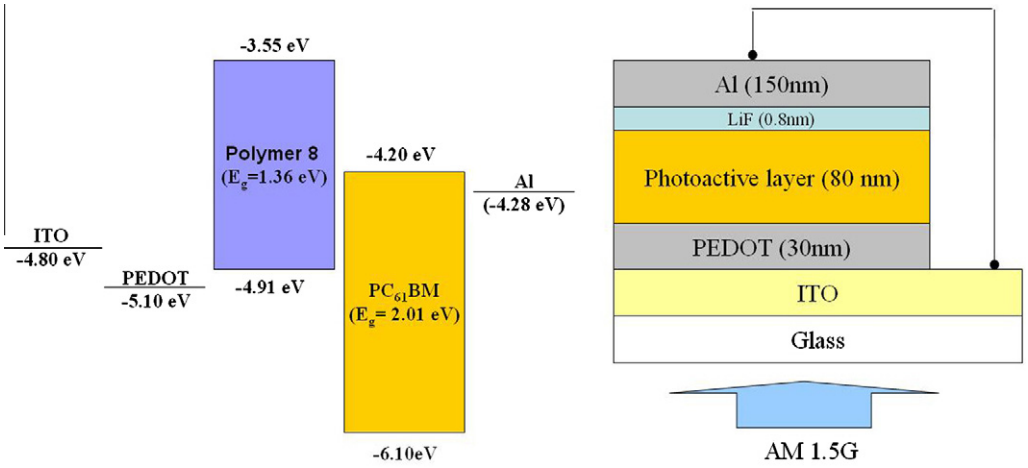

Fig. 7. Energy diagram of polymer photovoltaic cell (left). Device configuration of polymer solar cell (right).

in the accumulation mode of the polymer **8**-based TFTs. The output characteristics showed good saturation behaviors at low gate voltages, and clear saturation currents that were quadratic to the gate bias. The saturated field-effect mobilities, μ_{FET}, can be calculated from the amplification characteristics using the classical equations that describe field-effect transistors. The average mobility value obtained from five different devices equaled $(2.5 \pm 0.5) \times 10^{-3}$ cm^2/Vs with a current on/off ratio of approximately (1×10^2)–(3×10^2) and a threshold voltage, V_{th}, less than −15 V, under ambient conditions. The mobility value of the device fabricated using polymer **8** is comparable to those of D–A polymers for PSC, as reported in the literature [24].

The UV-induced photocrosslinking reaction is known to be detrimental to the semiconducting properties of the cell due to disruption of crystallization and molecular orderness [37]. It is noteworthy that a UV-induced crosslinked film of polymer **8** is very homogeneous and exhibits self-organization for uniform domains, which in turn enhances the ordered structure and charge transport in the thin film. Therefore, the mobility of the device made with the UV-cured film is comparable to that ($\mu = 3 \times 10^{-3}$ cm^2/Vs) of the device with unexposed film.

3.5. PSC device performances

PSC devices were fabricated by spin coating a solution of polymer **8**/$PC_{61}BM$ onto the PEDOT:PSS layer. After drying the blend film, the photocrosslinking reaction was induced using UV irradiation. The samples were exposed to UV light ($\lambda = 254$ nm, $I = 40$ mW/cm^2) for 20 min in order to cure the BHJ. The device configurations are as follows: ITO/PEDOT:PSS/polymer **8**:$PC_{61}BM$/LiF/Al (see Fig. 7).

Fig. 7 clearly illustrates the molecular energy levels and device configuration. First, PSC devices were fabricated using three polymer mixtures with $PC_{61}BM$ (1:1, 1:2, and 1:4 w/w). The characteristics of the device performances were determined under identical ambient conditions. The current density (J) versus voltage (V) curves of the PSCs are shown in Fig. 8. The devices **I**, **II**, and **III** contain photoactive layers with compositions of 1:1, 1:2, and 1:4 (polymer **8**:PCBM, w/w), respectively. The open-circuit voltage (V_{oc}), short-circuit current density (J_{sc}), fill factor (FF), and the PCE of the devices are summarized in Table 2. No significant change of the PCE was observed for the three different compositions, with all three samples displaying a PCE of almost unity ($\eta \approx 0.91$–1.08%). The effect of the annealing process on the device performances after annealing the samples at 80 °C followed by UV irradiation was also investigated. However, no significant annealing effects on the device performance accompanying the slight decrease of PCEs were observed. It appears that the photocuring effect is dominant over the thermal annealing effect, and manipulates the polymer structure toward the formation of ordered molecular structures in the PSCs. These preliminary experiments led us to select the blend ratio of 1:4 for further experiments to investigate the long-term stability of the PSCs.

In this experiment, the thermal annealing processes were excluded and the UV irradiation time was varied.

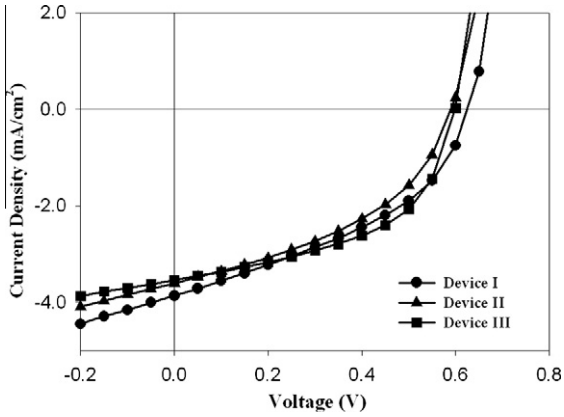

Fig. 8. Current density versus voltage curves of polymer **8**: $PC_{60}BM$ solar cells under AM 1.5G illumination. Circle: device **I**, triangle: device **II**, square: device **III**.

Table 2
Summary of polymer **8**-based PSC device performance.

Polymer **8**:PCBM (w/w)	J_{sc} (mA/cm^2)	V_{oc} (V)	FF	PCE (%)
1:1	−3.86	0.62	0.41	0.99
1:2	−3.61	0.59	0.43	0.91
1:4	−3.55	0.60	0.51	1.08

Fig. 9 shows the current density–voltage characteristics of the three devices under AM 1.5G illumination. The UV irradiation times were selected to be 0, 1, and 5 min at room temperature (see Table 3). Device **IV**, which was not UV irradiated ($t = 0$ min) demonstrated V_{oc}, J_{sc}, FF, and PCE values of 0.52 V, −3.35 mA/cm^2, 0.42, and 0.72%, respectively. The V_{oc} value (0.52 V) of device **IV** is smaller than the value shown in Fig. 8. For device **V**, in which the sample was exposed to UV light for 1 min, there was an increase in the J_{sc} value accompanied by an incremental increase in V_{oc}. The resultant PCE rose to 0.97% under these conditions. Finally, the sample that was irradiated for 5 min (device **VI**) had a PCE value of 1.37%, with increased J_{sc} and V_{oc} values relative to device **IV**. From the data, we concluded that a longer UV irradiation time leads to better device performance. In particular, the V_{oc} values varied with the irradiation time from 0.52 V for $t = 0$ min to 0.62 V for $t = 5$ min. In effect, the energy difference between the HOMO of the host polymer and the LUMO of the acceptor was found to most closely correlate with the V_{oc} value.

Theoretically, if the HOMO levels are identical, different devices having the same components should exhibit the same V_{oc} values regardless of the device conditions. These three samples exhibited inconsistent V_{oc} values, which could be attributed to the different surface morphological and interfacial properties between polymer **8** and $PC_{61}BM$, which could control the build-up potential.

In order to investigate the reason that device **III** showed the highest PCE value, the surface topographies of the blended films were observed using AFM microscopy. The AFM micrographs of the three samples are displayed in Fig. 10 along with the UV exposure time.

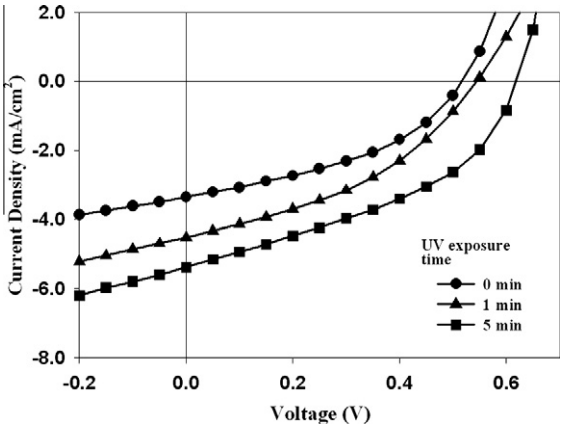

Fig. 9. Current density versus voltage curves of CP:$PC_{60}BM$ solar cells under AM 1.5G illumination. Device **IV**: pristine sample (circle); device **V**: UV exposure for 1 min (triangle); device **VI**: UV exposure for 5 min (square).

Table 3
Summary of polymer **8**-based PSC device performance with the UV exposure time.

Device	UV exposure time (min)	J_{sc} (mA/cm^2)	V_{oc} (V)	FF	PCE (%)
Device **IV**	0	−3.35	0.52	0.42	0.72
Device **V**	1	−4.52	0.54	0.39	0.97
Device **VI**	5	−5.37	0.62	0.41	1.37

From the three AFM images, it is easily noticeable that the surface topography changes with the UV exposure time. The pristine samples showed a surface roughness of 1.8–2.0 nm and contained a lot of large pinholes and dark areas. For longer irradiation times, the size of the pinholes significantly reduced and the surface became coarse. The sample exposed to UV light for 5 min has 8–10 nm surface roughness and the size of its pinholes is drastically reduced compared to the pristine sample. In principle, photopolymerization and the photocrosslinking reaction gave rise to the reduced volume of the polymer. It can be conjectured that under these conditions, the $PC_{61}BM$ domains were more tightly encompassed by polymer domains so that the interfacial contact could be highly improved. Therefore, more tightly bound polymer chains increase the short-circuit current (J_{sc}), resulting in increased PCE values. The reason for the increase in V_{oc} remains unclear in this study. A dense binary matrix has better interfacial contact that can reduce the build-up potential in the gap between the polymer and $PC_{61}BM$ domains.

Finally, we fabricated two devices; the first is the BHJ PSC cell made of P3HT and $PC_{61}BM$ (1:2 w/w), whereas the other is composed of polymer **8** and $PC_{61}BM$ (1:4 w/w). The latter was photocured by UV irradiation for 5 min under ambient conditions. The effect of photocrosslinking on the long-term stability of the devices was explored at 25 °C over a prolonged time period (t = 200 h). The decay behaviors of the PCEs are depicted in Fig. 11.

A P3HT:$PC_{61}BM$ (1:2 w/w) blended device was also prepared; it was not exposed to UV light and served as a control sample. The V_{oc}, J_{sc}, FF, and PCE values of the control sample were 0.60 V, 10.18 mA/cm^2, 0.60, and 3.79%, respectively. The photocured sample initially had V_{oc}, J_{sc}, FF, and PCE values of 0.65 V, 3.07 mA/cm^2, 0.47, and 0.97%, respectively. However, the photocured samples were quite different in terms of their long-term stability at ambient temperatures. The performance of the polymer **8**-based PSC devices treated with UV irradiation for 5 min were more stable in terms of device performance. In particular, the inset of Fig. 11 clearly showed slow decaying behavior of PCE of photocured sample in 40 h. Even after 200 h, the photocured devices retained more than 78% of the initial PCE. It was clearly observed in the inset of Fig. 11. In contrast, the device performance of the pristine-P3HT:$PC_{61}BM$ blend decreased rapidly to 25% of its initial efficiency value after 200 h. This result clearly shows that the photocrosslinking concept holds promise for thermally stable high-performance devices. All other evidence supports the efficacy of this synthetic strategy for improving the long-term stability of PSC device performance. Although we still observe a decreasing behavior for PSC device performance, the precise optimization of curing conditions and alternative methods for device fabrication may enhance the long-term stability of this polymer for fu-

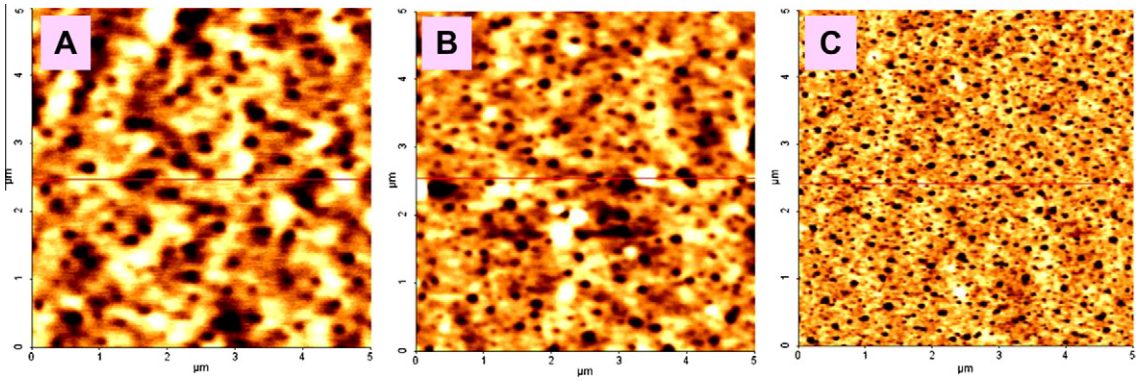

Fig. 10. AFM topographies of three film samples made of the polymer **8** deposited on PEDOT:PSS films. (A) Without UV exposure, (B) UV exposure for 1 min, (C) UV exposure for 5 min.

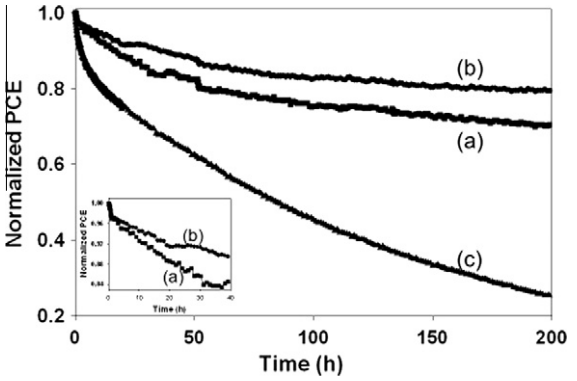

Fig. 11. Dynamic decaying behaviors of the PCE of PSCs under ambient conditions. (a) Polymer **8**:$PC_{61}BM$ before UV exposure, (b) polymer **8**:$PC_{61}BM$ after 5 min of UV exposure, and (c) P3HT:$PC_{61}BM$. Inset: expanded decaying behaviors of PCEs in 40 h.

ture use in practical applications. Our work unambiguously demonstrates that a photocrosslinkable and low-bandgap D–A alternating copolymer can be utilized for fabricating better PSC devices.

4. Conclusions

A soluble, photoreactive, low-bandgap D–A alternating copolymer based on cyclopentadithiophene and di(thiophen-2-yl)benzothiadiazole repeating units was synthesized by a palladium(0)-catalyzed Stille coupling reaction. The polymer contains pentadiene units in the side chain, which are reactive under UV exposure. A clear advantage of using the $PC_{61}BM$-containing polymer **8** in BHJ PSCs is that photocrosslinking can freeze the optimum internal morphology and long-term stability performance of the device can be achieved. Under optimized curing conditions, UV-cured polymer **8**-based PSC devices had a PCE of up to 1.37% under AM 1.5G illumination and the stability of PCE of photocured sample is better than the sample before UV exposure. BHJ solar cells based on the mixture of a D–A copolymer and $PC_{61}BM$ showed much improved long-term stability over long measuring periods as compared to conventional devices made of P3HT:$PC_{61}BM$.

These results can contribute to the design of photoreactive semiconducting π-conjugated polymers for practical applications in electronic and optoelectronic devices.

Acknowledgments

This research was supported by Korea Science and Engineering, (KOSEF R0120070001128402008) and by Priority Research Centers Program through the National Research Foundation of Korea (NRF) funded by the Ministry of Education, Science and Technology (NRF20100020209) Particularly, Prof. D.H. Choi thanks the financial support by the Seoul R&BD Program (10543, 2009–2010).

References

[1] M. Halik, H. Klauk, U. Zschieschang, G. Schmid, S. Ponomarenko, S. Kirchmeyer, W. Weber, Adv. Mater. 11 (2003) 917.
[2] J.A. Merlo, C.R. Newman, C.P. Gerlach, T.W. Kelley, D.V. Muyres, S.E. Fritz, M.F. Toney, C.D. Frisbie, J. Am. Chem. Soc. 127 (2005) 3997.
[3] H.E. Katz, Chem. Mater. 16 (2004) 4748.
[4] R.H. Friend, R.W. Gymer, A.B. Holmes, J.H. Burroughes, R.N. Marks, C. Taliani, D.D.C. Bradley, D.A.D. Santos, J.L. Bredas, M. Logdlund, W.R. Salaneck, Nature 397 (1999) 121.
[5] M.T. Bernius, M. Inbasekaran, J. O'Brien, W. Wu, Adv. Mater. 12 (2000) 1737.
[6] M.L. Chabinyc, A. Salleo, Y. Wu, P. Liu, B.S. Ong, M. Heeney, I. McCulloch, J. Am. Chem. Soc. 126 (2004) 13928.
[7] C.J. Brabec, N.S. Sariciftci, J.C. Hummelen, Adv. Funct. Mater. 11 (2001) 15.
[8] G. Yu, J. Gao, J.C. Hummelen, F. Wudl, A.J. Heeger, Science 270 (1995) 1789.
[9] L. Liu, C.-L. Ho, W.-Y. Wong, K.-Y. Cheung, M.-K. Fung, W.-T. Lam, A.B. Djurišić, W.-K. Chan, Adv. Funct. Mater. 18 (2008) 2824.
[10] H. Hoppe, N.S. Sariciftci, J. Mater. Chem. 16 (2006) 45.
[11] F.C. Krebs, H. Spanggaard, Chem. Mater. 17 (2005) 5235.
[12] J. Luo, Q. Hou, J. Chen, Y. Cao, Synth. Met. 156 (2006) 470.
[13] S.-P. Huang, J.-L. Liao, H.-E. Tseng, T.-H. Jen, J.-Y. Liou, S.-A. Chen, Synth. Met. 156 (2006) 949.
[14] D. Veldman, J.J.A.M. Bastiaansen, B.M.W. Langeveld-Voss, J. Sweelssen, M.M. Koetse, S.C.J. Meskers, R.A.J. Janssen, Thin Solid Films 511–512 (2006) 581.
[15] K. Chen, W.B. Caldwell, C.A. Mirkin, J. Am. Chem. Soc. 115 (1993) 1193.
[16] D.C. Coffey, O.G. Reid, D.B. Rodovsky, G.P. Bartholomew, D.S. Ginger, Nano Lett. 7 (2007) 738.
[17] M.M. Wienk, J.M. Kroon, W.J.H. Verhees, J. Knol, J.C. Hummelen, P.A.V. Hal, R.A.J. Janssen, Angew. Chem. Int. Ed. 42 (2003) 3371.
[18] G. Li, V. Shrotriya, J. Huang, Y. Yao, T. Moriarty, K. Emery, Y. Yang, Nat. Mater. 4 (2005) 864.
[19] W. Ma, C. Yang, X. Gong, K. Lee, A.J. Heeger, Adv. Funct. Mater. 15 (2005) 1617.
[20] S.A. Backer, K. Sivula, D.F. Kavulak, J.M.J. Fréchet, Chem. Mater. 19 (2007) 2927.
[21] J.Y. Kim, K. Lee, N.E. Coates, D. Moses, T.-Q. Nguyen, M. Dante, A.J. Heeger, Science 317 (2007) 222.
[22] M. Reyes-Reyes, K. Kim, D.L. Carroll, Appl. Phys. Lett. 87 (2005) 083506.
[23] J. Peet, J.Y. Kim, N.E. Coates, W.L. Ma, D. Moses, A.J. Heeger, G.C. Bazan, Nat. Mater. 6 (2007) 497.
[24] J. Hou, H.-Y. Chen, S. Zhang, G. Li, Y. Yang, J. Am. Chem. Soc. 130 (2008) 16144.
[25] J. Hou, H.-Y. Chen, S. Zhang, R.I. Chen, Y. Yang, Y. Wu, G. Li, J. Am. Chem. Soc. 131 (2009) 15586.
[26] Y. Liang, Z. Xu, J. Xia, S.-T. Tsai, Y. Wu, G. Li, C. Ray, L. Yu, Adv. Mater. 22 (2010) 1.
[27] B.J. Kim, Y. Miyamoto, B. Ma, J.M.J. Fréchet, Adv. Funct. Mater. 19 (2009) 2273.
[28] K. Sivula, Z.T. Ball, N. Watanabe, J.M.J. Fréchet, Adv. Mater. 18 (2006) 206.
[29] M. Drees, H. Hoppe, C. Winder, H. Neugebauer, N.S. Sariciftci, W. Schwinger, F. Schaffler, C. Topf, M.C. Scharber, Z. Zhu, R. Gaudiana, J. Mater. Chem. 15 (2005) 5158.
[30] Z. Zhu, S. Hadjikyriacou, D. Waller, R. Gaudiana, J. Macromol. Sci. Part A Pure Appl. Chem. 41 (2004) 1467.
[31] E. Zhou, Z.A. Tan, C. Yang, Y. Li, Macromol. Rapid Commun. 27 (2006) 793.
[32] H. Wynberg, A. Kraak, J. Org. Chem. 29 (1964) 2455.
[33] M. Jayakannan, P.A. Van Hal, R.A.J. Janssen, J. Poly. Sci. Part A: Poly. Chem. 40 (2002) 2360.
[34] H. Kim, J.Y. Kim, K. Lee, Y. Park, Y. Jin, H. Suh, Curr. App. Phys. 1 (2001) 139.
[35] M. Theander, A. Yartsev, D. Zigmantas, V. Sundström, W. Mammo, M.R. Andersson, O. Inganäs, Phys. Rev. B 61 (2000) 12957.
[36] F. Meng, J. Hua, K. Chen, H. Tian, L. Zuppiroli, F. Nuesch, J. Mater. Chem. 15 (2005) 979.
[37] I. McCulloch, W. Zhang, M. Heeney, C. Bailey, M. Giles, D. Graham, M. Shkunov, D. Sparrowe, S. Tierney, J. Mater. Chem. 13 (2003) 2436.